This article has been accepted for publication in IEEE Transactions on Antennas and Propagation. This is the author's version which has not been fully edited and content may change prior to final publication. Citation information: DOI 10.1109/TAP.2024.3467677

C-/Ka-Band Low-Profile Circularly Polarized Shared-Aperture Antenna for CubeSat Communications

Zhichao Sun, Zhenxi Liang, Xiaojing Lv, *Member, IEEE,* Yonggang Zhou, *Member, IEEE,* Shaobin Liu, *Member, IEEE*, Zhen Luo, and Yang Yang, *Senior Member, IEEE*

***Abstract*—This communication presents a low-profile circularly polarized (CP) shared-aperture antenna at *C*- and *Ka*-band for CubeSat communications. It consists of a *C*-band metasurface antenna and a 4×4 *Ka*-band magnetoelectric (ME) dipole antenna array, and only has 0.057λ_{low} thickness. The square ring reactive impedance surface (RIS) and an irregularly shaped driven patch are meticulously designed in the *C*-band antenna without affecting the radiation performance of the *Ka*-band antenna. Meanwhile, a sequential rotation feeding network (SRFN) is adopted for the *Ka*-band antenna to improve the axial ratio (AR) performance. The measured results show that the overlapped operational bands (|S_{11}| < -10 dB, AR < 3 dB) are 11.4% (6.2-6.95 GHz) for the C-band and 36.7% (26-37.7 GHz) for the Ka-band, with realized peak gains of 9.36 dBic and 17.2 dBic, respectively. The isolations of the shared aperture antenna within the two operating bandwidths are both better than 20 dB. With the excellent advantages of low-profile and dual-wideband, the proposed antenna is suitable for various communication applications in CubeSats.**

***Index Terms*—CubeSat, circularly polarized (CP), shared-aperture, low-profile, Magnetoelectric (ME) dipole antenna**

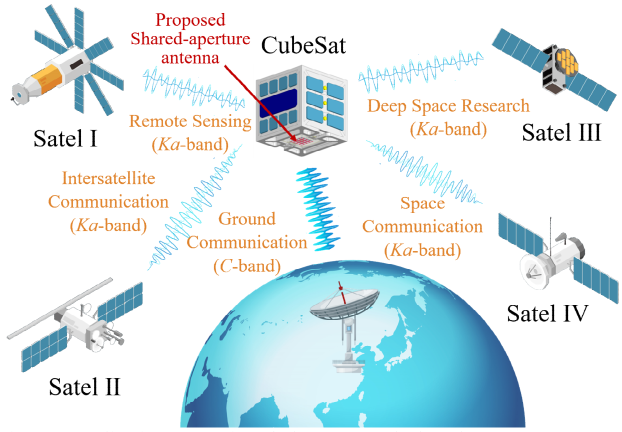

Fig. 1. Application scenario of the proposed shared-aperture antenna in CubeSat.

I. INTRODUCTION

In recent years, CubeSats have emerged as a significant innovation in nanosatellites. Characterized by their standardized dimensions, CubeSats are typically constructed in units denoted as "U". A single CubeSat unit (1U) measures 10×10×10cm^3, with larger configurations realized by combining multiple units [1]. The primary advantages of CubeSats include their low production costs, diminutive size, rapid development cycles, and the flexibility afforded by their modular design. These attributes have catalyzed their extensive use in various space missions, encompassing inter-satellite communication, remote sensing, space communication, and deep space research [2].

In current CubeSat antenna systems, multiple antennas operating in different frequency bands are required in CubeSats to conduct various scientific research missions. Integrating multiple broadband and high-gain antennas within CubeSats' limited volume and weight constraints presents a significant challenge [3]. Recently, several innovative antennas, such as inflatable antennas [4-6], deployable reflectarray (RA) antennas, and mesh reflector antennas [7-11], have been developed for CubeSats. These antennas offer high realized gains and can be stored within the CubeSat. However, they face limitations such as poor surface accuracy, large stowage requirements (>1.5U), and mechanical complexity. Once these antennas are mounted, there is little space left in CubeSats for additional antennas. Therefore, implementing shared-aperture technology that supports dual- or tri-band functionality within the same aperture is a promising solution.

Until now, various novel aperture-shared antennas comprising planar antennas [12-22], waveguide antennas [23-25], and RA antennas [26], [27] have been reported are appropriate for satellite communications. The planar shared-aperture antennas, such as Fabry-Perot (FP) resonator antenna [12-15], microstrip patch antennas [16-20], and substrate integrated waveguide (SIW) antennas [21], [22], are easily implemented on low-profile dielectric substrates, in which the key issue is the tradeoff between size and bandwidth. Considering the various spurious signals in Low Earth Orbit (LEO) and communication reliability, wide operating bandwidth is significant for CubeSat antennas. In response to the rapid movement of CubeSats in space, numerous metal waveguide shared-aperture antennas have been developed [23-25]. These antennas have extremely high mechanical strength, allowing for stable operation, but they are only suitable for medium and large satellites due to their large size and heavy weight. Reflect-arrays, as proposed in [26] and [27], achieve high gains and high-frequency ratios but require an additional feed, which creates installation challenges. Additionally, both types of antennas exhibit linear polarization (LP), which can lead to polarization mismatches between transmitting and receiving antennas [28]. Therefore, designing a lightweight, low-profile, dual-wideband circularly polarized (CP) shared-aperture antenna remains a significant challenge to meet the small size and multifunctional requirements of CubeSats.

This work was supported by University of Technology Sydney ARC Future Fellow Near Miss Support Grant (*Corresponding author: Yang Yang*)

Zhichao Sun is with the College of Electronic and Information Engineering, Nanjing University of Aeronautics and Astronautics, Nanjing, 210016, China, and also with the School of Electrical and Data Engineering, University of Technology Sydney, Sydney, NSW 2019, Australia.

Xiaojing Lv and Zhen Luo are with the School of Mechanical and Mechatronic Engineering, University of Technology Sydney, Sydney, NSW 2019, Australia.

Yonggang Zhou and Shaobin, Liu is with the College of Electronic and Information Engineering, Nanjing University of Aeronautics and Astronautics, Nanjing, 210016, China.

Zhenxi Liang, and Yang Yang are with the School of Electrical and Data Engineering, University of Technology Sydney, Sydney, NSW 2019, Australia.

(e-mail: bryan068@nuaa.edu.cn, Zhenxi.Liang@student.uts.edu.au, xiaojing.lv@uts.edu.au, zyg405@nuaa.edu.cn, lsb@nuaa.edu.cn, zhen.luo@uts.edu.au, yang.yang.au@ieee.org).

This article has been accepted for publication in IEEE Transactions on Antennas and Propagation. This is the author's version which has not been fully edited and content may change prior to final publication. Citation information: DOI 10.1109/TAP.2024.3467677

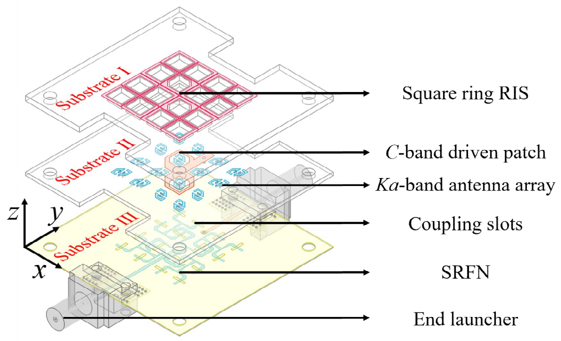

Fig. 2. Isometric view of the proposed shared-aperture antenna.

This work proposes a low-profile CP shared-aperture antenna for CubeSat applications. The *C*- and *Ka*-band are selected as the operating band. The former has excellent penetration and long-distance communication capabilities and is widely used in ground communication. The latter is employed for various space missions owing to its high data transmission rates. The application scenario is depicted in Fig. 1. For high gain and wideband CP performance, the square ring reactive impedance surface (RIS) and the irregularly shaped patch are adopted as the radiation part and driven patch for the *C*-band antenna, respectively. The 4×4 *Ka*-band antenna array is integrated into the *C*-band antenna and shares the same aperture. A sequential rotation feeding network (SRFN) is developed for the *Ka*-band to overcome the deterioration of AR with increased sub-array distance. The entire antenna is only 0.057λ_{low} thickness with a large frequency ratio. An antenna prototype and a 3-D printed CubeSat platform are fabricated for performance verification.

II. Antenna Configuration and Operation Principle

Fig. 2 shows the configuration of the proposed shared-aperture antenna. It consists of three substrates and integrated by screws. Both feeding networks are printed on the bottom of the Substrate III (Taconic TLY-5, 0.254mm), while the feeding microstrip of the *C*-band antenna is connected to the driven patch on Substrate II (Taconic TLY-5, 1.016mm) by metal vias. The *Ka*-band antenna array is printed on Substrate II, and the metasurfaces are on Substrate I (Taconic TLY-5, 1.524mm), respectively. To prevent interference with the radiation of the *Ka*-band antenna, part of the Substrate I above the *Ka*-band antenna array is hollowed out.

A. Ka-band Antenna Element and Working Principle

The *Ka*-band antenna element is shown in Fig. 3. The radiation structure is composed of a pair of bent stubs and is connected to the ground with four metallic vias. A microstrip feeding line is mounted on the bottom substrate to feed the element. The slot between the radiators and the vias is equipped as the magnetic dipole, and the stubs work as the electric dipole. The electric dipole and magnetic dipole work in parallel as a complementary source, composing the ME-dipole antenna. Considering the couplings between other elements in the array, periodic boundaries are set in the *x*- and *y*-directions. The detailed parameter values are given in Fig. 3.

Fig. 4 presents the simulated results of the proposed *Ka*-band antenna element. The antenna exhibits a -10 dB impedance bandwidth of 41.27% (25-38 GHz), a 3-dB AR bandwidth of 36.99% (27.1-39.4 GHz), and a peak realized gain of 8.25 dBic. The overlapped bandwidth is 27.1-38 GHz (33.5%), demonstrating the wideband CP performance. The normalized antenna radiation patterns in *xoz*- and *yoz*-planes at 30 GHz and 36 GHz are shown in Fig. 5. Benefiting from

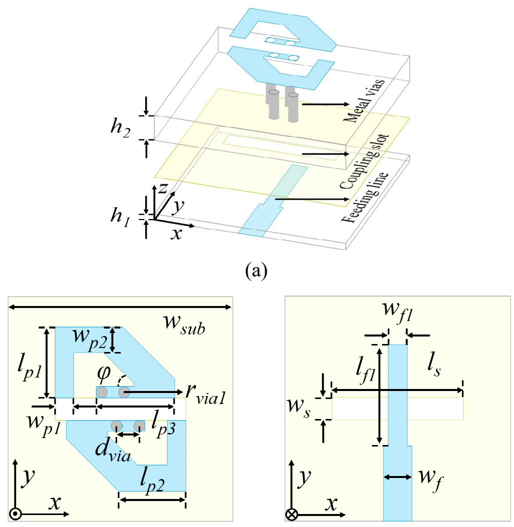

Fig. 3. Geometry of the proposed Ka-band antenna element. (a) 3-D view, (b) top view and bottom view. (h_1=0.254, h_2=1.016, w_{sub}=6, l_{p1}=1.9, l_{p2}=1.8, l_{p3}=2.1, w_{p1}=0.5, w_{p2}=0.7, d_{via}=0.6, r_{via1}=0.15, φ=45°, l_s=3.5, w_s=0.6, l_{f1}=2.7, w_{f1}=0.5, w_f=0.75 (unit: mm)).

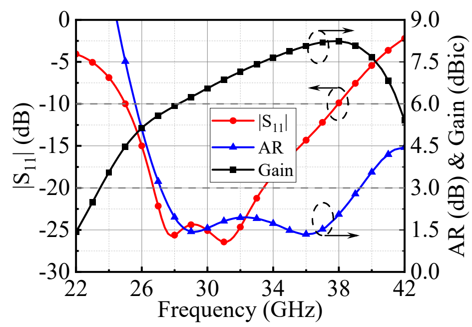

Fig. 4. Simulated reflection coefficient, AR and realized gain of the proposed *Ka*-band antenna element.

the excellent radiation performance of ME-dipole antenna, the antenna element radiated stably and realized low cross-polarization levels in the operating bandwidth.

Fig. 6 depicts the current distributions on the bent stubs at the center frequency of 33 GHz. It can be seen that the current is mainly concentrated at the first transverse stub and the oblique stub. At time t=0 and T/2, the main current distributions on the patches are along the -*x*-direction and opposite. The vector currents change to *x*-direction with around -45° and 135° at t=T/4 and 3T/4, respectively. Consequently, the surface current rotates counterclockwise, demonstrating that RHCP performance is realized.

B. Development of C-band Antenna

The *C*-band antenna consists of a driven patch and a 4×4 metasurface array. In the study of [29], the lattice of square metal plates called reactive impedance surface (RIS) above the driven patch can generate extra resonance at a particular frequency, which enhances the performance of the antenna. The square ring RIS and irregularly shaped driven patch are utilized to integrate the *C*- and *Ka*-band antennas into the same aperture. The chamfer square patch is typically adopted as the CP radiator or driven component. Still, it is not applicable in this design because it will block the radiation of the Ka-band antenna and cause a strong coupling between them. Therefore, we first hollowed out the chamfer square patch along the square ring

This article has been accepted for publication in IEEE Transactions on Antennas and Propagation. This is the author's version which has not been fully edited and content may change prior to final publication. Citation information: DOI 10.1109/TAP.2024.3467677

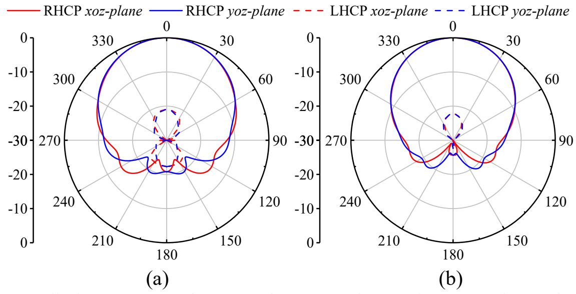

Fig. 5. Radiation patterns of proposed antenna element in *xoz*- and *yoz*-planes at 30 GHz and 36 GHz.

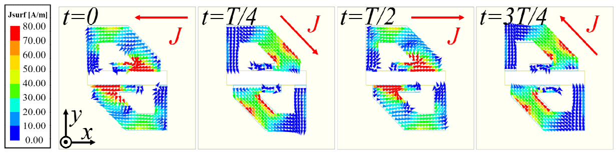

Fig. 6. Simulated current distributions at 33 GHz at different times.

RIS, as shown in step 1 in Fig. 7. However, the AR performance deteriorates with the current path on the patch being cut off. To expand the AR bandwidth of the *C*-band antenna, the slots on the driven patch are designed in a smaller chamfer square, and RISs above the driven patch are also developed into the same shape, illustrated in step 2. As shown in Fig. 8(a), the AR bandwidth of the proposed antenna increased by 6% compared with the simple hollowed driven patch. Fig. 8(b) illustrates the radiation pattern of the proposed *C*-band antenna at 6.5 GHz. The proposed antenna exhibits the RHCP radiation performance, and the simulated realized gain is 9.5 dBic, with the cross-polarized level being less than 20 dB.

C. Shared-Aperture Antenna Design

A full-corporate feeding network is usually adopted in the wideband CP antenna array [30], [31]. However, the AR bandwidth of the array will inevitably decrease when this feeding network is applied. Thus, the sequential rotation feeding network (SRFN) is designed to introduce an additional CP mode [32]. It rotates clockwise/anticlockwise and a 90° phase difference along the clockwise/anticlockwise direction was realized. Compared with the full-corporate feeding network, the SRFN can mitigate the adverse AR influences caused by such as excessive array spacing or poor axial ratio performance of individual elements.

Nevertheless, there is insufficient space for the arrangement of the SRFN when the element spacing in the array remains the same as the w_{sub}. Therefore, it is necessary to expand the size of the 2×2 subarray. The optimized subarray is shown in Fig. 9(a). A tapered 1-to-4 power divider is utilized for constant amplitude and in-phase feed. The side length of the subarray is 12.8 mm, which is greater than twice that of the element. The simulated results of the subarray are shown in Fig. 9(b). It is observed that the impedance bandwidth and AR bandwidth are slightly deteriorated compared with the element. This also demonstrates that it is necessary to feed with an SRFN.

To investigate the effect of RIS on the *Ka*-band antenna array, the 4×4 antenna array w/o and with RIS are simulated. As inserted in Fig. 10, four subarrays are rotated sequentially around the axial center and fed with an SRFN. The simulated results in Fig. 10(a) show that the overlapped bandwidth is 40% (24-36 GHz), which increased by 6.5% compared with that of the element, and the peak realized gain is 18.1 dBic at 32 GHz. Fig. 10(b) illustrates the simulated result incorporating the 4×4 antenna array with the RIS. Compared with the non-RIS-loaded array, only the realized gain slightly reduced after

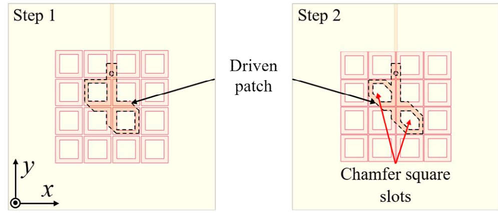

Fig. 7. Develop process of the proposed *C*-band antenna.

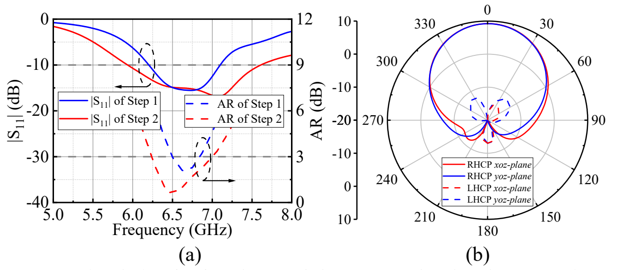

Fig. 8. (a) Simulation $|S_{11}|$ and AR of the proposed *C*-band antenna in two steps, (b) radiation patterns of the *C*-band antenna at 6.5 GHz in Step 2.

32.5 GHz, remaining within an acceptable range.

Based on the proposed *C*- and *Ka*-band antenna, the shared-aperture antenna is developed and optimized, as depicted in Fig. 11. The entire PCB is extended to 50×50 mm^2 to reduce the influence of the *Gwave* millimeter wave connector. To minimize the obstruction of the *Ka*-band array by RIS, the inner side length of the square ring (w_{p3}) was enlarged by 0.6 mm. The driven patch is printed between the *Ka*-band array on Substrate II, which is connected to the 50 Ω feeding microstrip by a metal via passing through the Substrate II and III. The radius of the isolation hole (r_{via3}) on the ground is twice the radius of the metal via (r_{via2}). Tapered microstrip lines are selected as impedance transformers in the *Ka*-band feeding network, and cuts at the corners are utilized for better impedance matching [41]. The detailed parameter values are listed in Fig. 11. Fig. 12 depicts the simulated reflection coefficients, AR, and realized gains of the shared-aperture antenna. The overlapped bandwidth is 10.3% and 31.56% at *C*- and *Ka*-band, respectively. The simulated peak gain is 9.3 dBic at the *C*-band and 17.8 dBic at the *Ka*-band. It is evident that the bandwidth and gain inevitably experience degradation after integrating the *C*- and *Ka*-band antenna into the same aperture, while the shared-aperture antenna still maintains wideband CP performance.

The current distributions on RIS, driven patch, and *Ka*-band arrays are shown in Fig. 13. The superimposed vector current *J* on the RIS and driven patch rotates counterclockwise over the whole period *T*, and the RHCP radiation performance is generated. In addition, the current on the *Ka*-band array is very weak. To exhibit the dual-band performance more intuitively, Fig. 14 shows the *E*-field distributions of the shared-aperture antenna at two frequency bands. At the *C*-band, the driven patch is operated while the *Ka*-band array is inactive. Conversely, only the *Ka*-band array produces the radiation at the *Ka*-band and the *E*-field on the driven patch is very weak. The *E*-field distributions validate that the shared-aperture antenna is capable of operating individually at *C*- and *Ka*-band with extremely low mutual coupling.

III. Results and Discussion

A. Simulated and Measured Results

A prototype of the shared-aperture antenna is fabricated to verify the performance, as shown in Fig. 15(a). Three substrates are separately

This article has been accepted for publication in IEEE Transactions on Antennas and Propagation. This is the author's version which has not been fully edited and content may change prior to final publication. Citation information: DOI 10.1109/TAP.2024.3467677

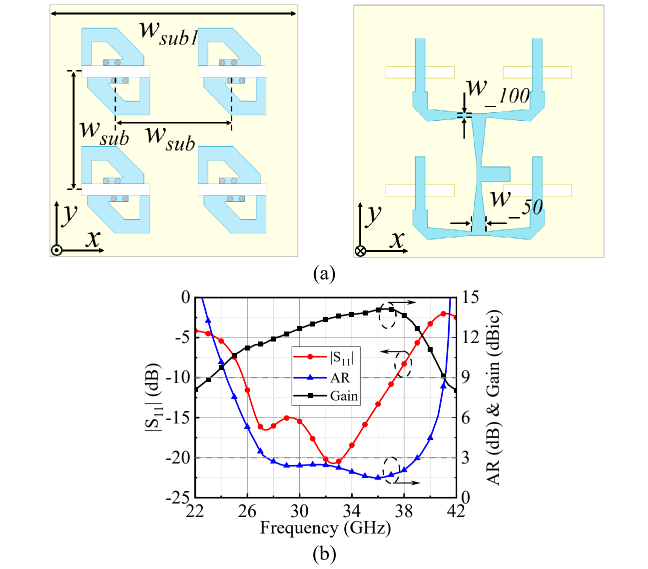

(a)

(b)

Fig. 9. (a) Geometry of the proposed *Ka*-band subarray, (b) Simulated reflection coefficient, AR and realized gain of the proposed subarray. (w_{sub1}=12.8, $w_{\_100}$=0.2, $w_{\_50}$=0.75 (unit: mm))

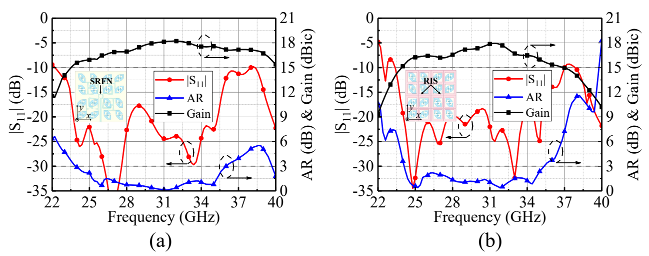

(a)

(b)

Fig. 10. Simulated results of the 4×4 Ka-band array (a) w/o RIS, (b) with RIS.

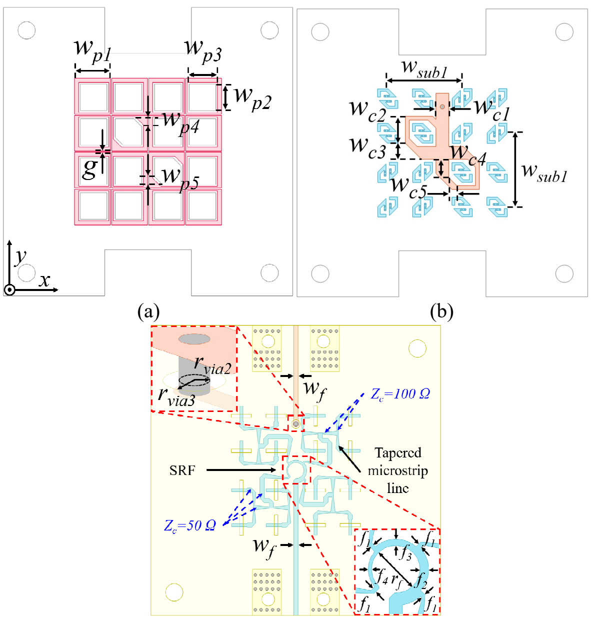

(a)

(b)

(c)

Fig. 11. Geometry of the proposed shared-aperture antenna. (a) Substrate I, (b) Substrate II, (c) Substrate III. (w_{p1}=6.2, w_{p2}=4.6, w_{p3}=5.2, w_{p4}=1.38, w_{p5}=1.38, g=0.2, w_{c1}=2.2, w_{c2}=4.7, w_{c3}=2.75, w_{c4}=3.22, w_{c5}=1.38, r_{via2}=0.375, r_{via3}=0.75, f_1=0.25, f_2=0.45, f_3=0.38, f_4=0.2, r_f=1 (unit: mm)).

manufactured and fixed with four screws. A tin wire is used to connect the metal vias on Substrate II and III and soldered for stable electrical

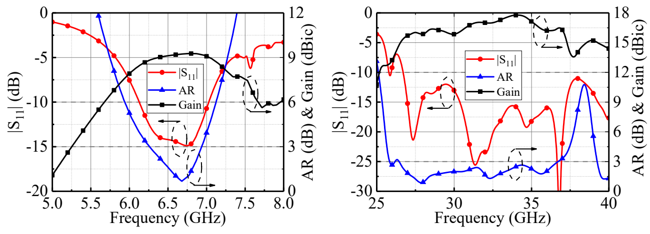

(a)

(b)

Fig. 12. Simulated results of (a) *C*-band antenna, (b) *Ka*-band antenna array.

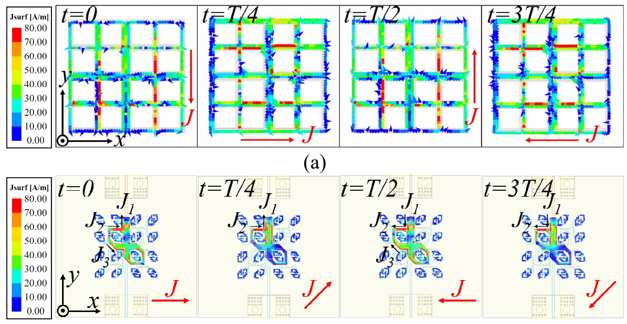

(a)

(b)

Fig. 13. Simulated current distributions on (a) RIS, (b) driven patch and *Ka*-band array at 6.5 GHz.

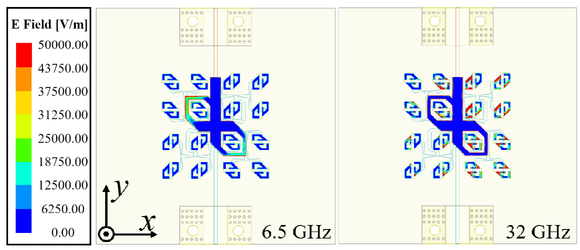

Fig. 14. *E*-field distributions on the surface of Substrate II of shared-aperture antenna at 6.5 GHz and 32 GHz.

connection. Two *Gwave* end-launcher connectors are applied for measurement. Meanwhile, a 1U CubeSat platform is introduced for simulation and measurement, as depicted in Fig. 15(b) and the bottom right corner of (c). The proposed shared-aperture antenna can be conveniently mounted on it. The reflection coefficients are measured by a Keysight N5225B network analyzer and the radiation performance is experimented in a microwave anechoic chamber, the measurement setup is shown in Fig. 15(c).

The simulated and measured S-parameters, ARs, and realized gains are shown in Fig. 16. It can be observed that the measured -10 dB impedance bandwidth is 16.5% (6.1-7.2 GHz) and 36.7% (26-37.7 GHz) at *C*-band and *Ka*-band, respectively. Besides, the isolations between the two ports maintain a high level which is both below -20 dB. The simulated and measured 3 dB AR bandwidth of the *C*-band antenna is 10.3% covering 6.26-6.94 GHz and 11.4% (6.2-6.95 GHz), and that of the *Ka*-band antenna is 32.55% (26.44-36.72 GHz) and 39.37% (25.5-38 GHz). The measured overlapped bandwidth of the two bands is 11.4% and 36.7%, and the measured peak gain is 9.36 dBic and 17.2 dBic, respectively. Fig. 17 presents the simulated and measured normalized radiation patterns at 6.5, 28, and 34 GHz. Stable RHCP radiation patterns are realized within both operating bandwidths. Notably, the 160° to 200° range constitutes a blind area due to the presence of absorbing material positioned behind the antenna mount, as shown in the bottom left corner of Fig. 15(c). Overall, the simulated and measured results are in good agreement and the little discrepancies may be caused by the deviations during the

This article has been accepted for publication in IEEE Transactions on Antennas and Propagation. This is the author's version which has not been fully edited and content may change prior to final publication. Citation information: DOI 10.1109/TAP.2024.3467677

TABLE I
COMPARISON OF DIFFERENT SHARED-APERTURE ANTENNAS SUITABLE FOR SATELLITE COMMUNICATION

Ref.	Operation Bands	IMBW (%)	ARBW (%)	Antenna type	Profile (λ_{low})	Polarization	Gain (dBic)	Frequency ratio
12	UHF/C	3.9/9.9	1.0/4.0	Patch + FP resonator cavity	0.075	CP	5.8/13.8	6.4
14	X/Ka	4/4.5	-	FP resonator cavity + TA	0.57	LP	13.8/23.6	2.775
16	X/Ku	8.3/18.9	14.2/14.9	Microstrip patch	0.024	CP	17.45/18.26	1.43
19	C/X	21/21.2	13.2/12.8	Coupling slot + patch	0.077	CP	14.5/17.5	1.55
20	X/Ka	2.9/3.6	-	Microstrip dipole	0.05	LP	12.8/20.1	3.1
21	X/Ku	12/10.5	4.3/4.9	Patch + SIW Rotman lens	0.24	CP	21.3/21.9	1.22
22	C/X	4.5/2.7	1.04/0.75	SIW + Microstrip	0.048	CP	8.4/6.35	1.61
23	Ku/Ka	19.4/7.4	-/7.4	QCWL + HW	2.8	LP/CP	18.4/23.4	2.1
24	K/Ka	20/13.3	20/13.3	CP waveguide	4.7	CP	23.94/26.87	1.5
26	S/Ka	6/20	-	Patch + RA	0.05	LP	13.7/27.65	7.37
27	X/Ka	45/11.4	-	Coupling slots + RA	-	LP	21.7/30.1	3.1
This work	**C/Ka**	**16.5/36.7**	**11.4/39.37**	**RIS + ME-dipole**	**0.057**	**CP**	**9.36/17.2**	**4.8**

FP: Fabry-Perot; TA: transmitarray; QCWL: quasi-planar coaxial waveguide line; HW: hollow-waveguide; RA: reflectarray;

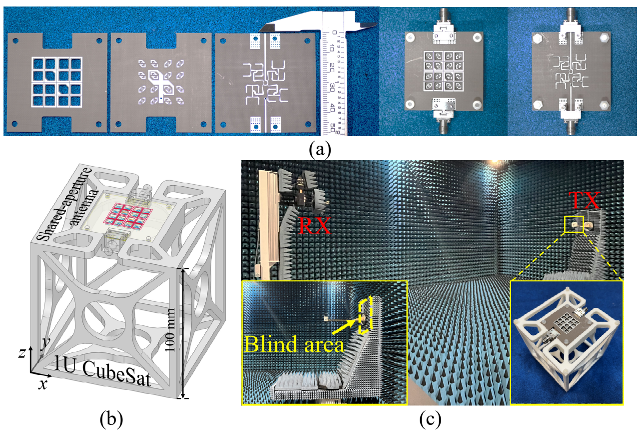

Fig. 15. (a) Photograph of the fabricated antenna prototype, (b) configuration of the simulation model, (c) photographs of the measurement set up and fabricated platform with antenna prototype.

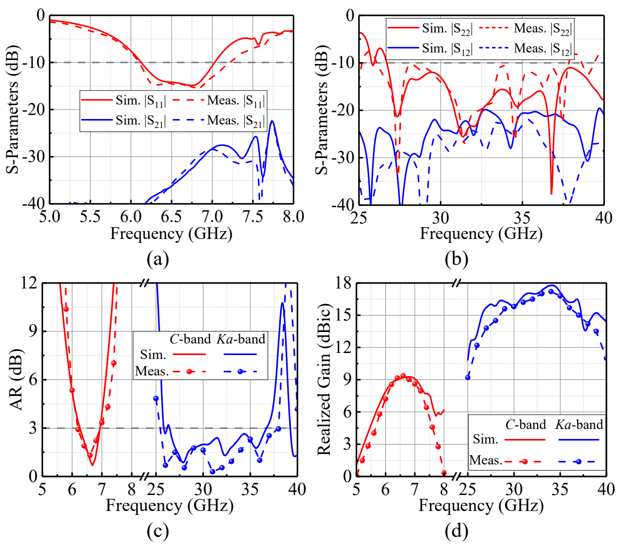

Fig. 16. Simulated and measured results of the proposed antenna. S-parameters at (a) *C*-band, (b) *Ka*-band. (c) AR, (d) realized gain.

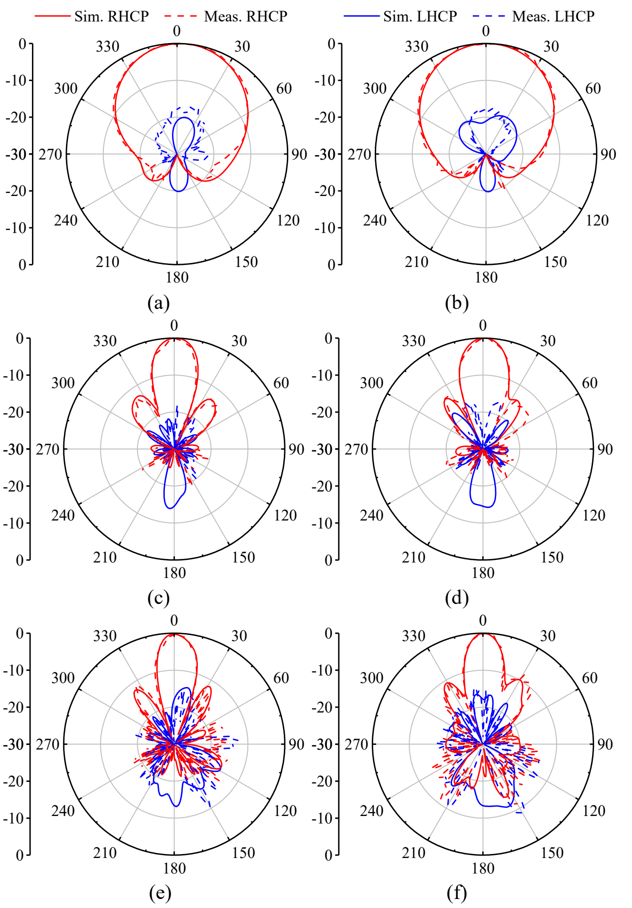

Fig. 17. Simulated and measured normalized radiation patterns. (a) *xoz*-plane at 6.5 GHz, (b) *yoz*-plane at 6.5 GHz, (c) *xoz*-plane at 28 GHz, (d) *yoz*-plane at 28 GHz, (e) *xoz*-plane at 34 GHz, (f) *yoz*-plane at 34 GHz.

assembly process, tolerance of the material loss tangent, and measurement errors.

B. Comparison and Discussion

Table I summarizes the key performance metrics between the proposed antenna and other shared-aperture antennas appropriate for satellite communications. In [12], a mesh structure is developed to function as a microstrip CP antenna at the UHF band and works as an FP resonator cavity at the *C*-band. Although a low profile and high-frequency ratio is realized, the bandwidth is insufficiently addressed, potentially making it susceptible to interference from other signals and thereby reducing communication reliability. Various planar shared-aperture antenna such as microstrip antenna, and transmitarray with compact sizes are reported in [14] and [20]. However, only LP has been achieved, which may result in polarization mismatch. Although compact CP antennas are implemented in [16],

This article has been accepted for publication in IEEE Transactions on Antennas and Propagation. This is the author's version which has not been fully edited and content may change prior to final publication. Citation information: DOI 10.1109/TAP.2024.3467677

[19], [21], and [22], the frequency ratio is below two or operated in the same frequency band. Metal waveguides with exceptional mechanical strength have been effectively utilized to withstand high-speed operations in space, as reported in [23] and [24]. However, the heavyweight restricts their applications to nanosatellites. To address long-distance communications between satellites, two RAs with high realized gain have been designed in [26] and [27], while an additional feeding source is necessary which may present installation challenges.

IV. Conclusion

A low-profile CP shared-aperture antenna operated at *C*- and *Ka*-band is proposed in this communication. The *C*-band metasurface antenna utilized square ring RIS and optimized driven patch, exhibiting stable CP radiation performance. The SRFN is developed for the *Ka*-band antenna array to enhance the AR performance. An antenna prototype is fabricated and measured to verify the design concept. The measured overlapped bandwidth in terms of -10 dB reflection coefficients and 3 dB AR is 11.4% and 36.7% at *C*- and *Ka*-band, respectively. The measured peak gain is 9.36 dBic at the *C*-band and 17.2 dBic at the *Ka*-band. Moreover, it can be easily turned into dual-CP by mirroring the structure, or expanded to a large array for higher gain. Overall, the proposed antenna with low-profile, dual-band, medium gain, and lightweight provides an attractive solution with wide CP performance in limited size, which is a desirable communication antenna in CubeSats.

References

[1] *What are SmallSats and CubeSats?* [Online] Available: https://www.nasa.gov/what-are-smallsats-and-cubesats/.
[2] R. Baktur, Antenna Design for CubeSat, Artech, 2021, ch. 1.
[3] F. E. M. Tubbal, R. Raad, K.-W. Chin, and B. Butters, "S-band planar antennas for a CubeSat," *Int. J. Electr. Eng. Informat.*, vol. 7, no. 4, pp. 559-568, Dec. 2015.
[4] A. Babuscia, M. Van de Loo, Q. J. Wei, S. Pan, S. Mohan, and S. Seager, "Inflatable antenna for cubesat: fabrication, deployment and results of experimental tests," in *2014 IEEE Aerospace Conf.*, Big Sky, MT, USA, 2014, pp. 1-12.
[5] A. Babuscia, T. Choi, J. Sauder, A. Chandra, and J. Thangavelautham, "Inflatable antenna for CubeSats: Development of the X-band prototype," *in Proc. IEEE Aerosp. Conf.*, Big Sky, MT, USA, Mar. 2016, pp. 1-11
[6] A. Babuscia, J. Sauder, A. Chandra, J. Thangavelautham, L. Feruglio, and N. Bienert, "Inflatable antenna for CubeSat: A new spherical design for increased *X*-band gain," in *Proc. IEEE Aerosp. Conf.*, Big Sky, MT, USA, Mar. 2017, pp. 1-10.
[7] R. E. Hodges, D. J. Hoppe, M. J. Radway, and N. E. Chahat, "Novel deployable reflectarray antennas for CubeSat communications," in *2015 IEEE MTT-S International Microwave Symposium*, Phoenix, AZ, USA, 2015, pp. 1-4.
[8] M. W. Nichols, A. Gonzalez, E. A. Alwan, and J. L. Volakis, "An Accordion-Folding Series-Fed Patch Array With Finite Thickness: A folding technique for CubeSat arrays," *IEEE Antennas and Propag. Magazine*, vol. 65, no. 3, pp. 77-82, June 2023.
[9] N. Chahat, J. Sauder, M. Mitchell, N. Beidleman, and G. Freebury, "One-Meter Deployable Mesh Reflector for Deep-Space Network Telecommunication at X-Band and Ka-Band," *IEEE Trans. Antennas Propag.*, vol. 68, no. 2, pp. 727-735, Feb. 2020.
[10] N. Chahat, R. E. Hodges, J. Sauder, M. Thomson, E. Peral, and Y. Rahmat-Samii, "CubeSat Deployable Ka-Band Mesh Reflector Antenna Development for Earth Science Missions," *IEEE Trans. Antennas Propag.*, vol. 64, no. 6, pp. 2083-2093, June 2016.
[11] R. E. Hodges, M. J. Radway, A. Toorian, D. J. Hoppe, B. Shah, and A. E. Kalman, "ISARA-integrated solar array and reflectarray CubeSat deployable Ka-band antenna," in *Proc. IEEE Antennas Propag. Soc. Int. Symp.*, Vancouver, BC, Canada, Jul. 2015, pp. 2141-2142.
[12] C. Chen, "A Dual-Band Circularly Polarized Shared-Aperture Antenna for 1U CubeSat Applications," *IEEE Trans. Antennas Propag.*, vol. 70, no. 5, pp. 3818-3823, May 2022.
[13] T. Li and Z. N. Chen, "Shared-Surface Dual-Band Antenna for 5G Applications," *IEEE Trans. Antennas Propag.*, vol. 68, no. 2, pp. 1128-1133, Feb. 2020.
[14] P. Mei, S. Zhang, and G. F. Pedersen, "A Dual-Polarized and High-Gain X-/Ka-Band Shared-Aperture Antenna With High Aperture Reuse Efficiency," *IEEE Trans. Antennas Propag.*, vol. 69, no. 3, pp. 1334-1344, March 2021.
[15] J. Zhu, Y. Yang, S. Liao, S. Li, and Q. Xue, "Dual-Band Aperture-Shared Fabry-Perot Cavity-Integrated Patch Antenna for Millimeter-Wave/Sub-6 GHz Communication Applications," *IEEE Antennas and Wireless Propag. Letters*, vol. 21, no. 5, pp. 868-872, May 2022.
[16] J. D. Zhang, W. Wu, and D. G. Fang, "Dual-Band and Dual-Circularly Polarized Shared-Aperture Array Antennas With Single-Layer Substrate," *IEEE Trans. Antennas Propag.*, vol. 64, no. 1, pp. 109-116, Jan. 2016.
[17] M. J. Veljovic and A. K. Skrivervik, "Aperture-Coupled Low-Profile Wideband Patch Antennas for CubeSat," *IEEE Trans. Antennas Propag.*, vol. 67, no. 5, pp. 3439-3444, May 2019.
[18] Y. Yao, S. Liao, J. Wang, K. Xue, E. A. Balfour, and Y. Luo, "A New Patch Antenna Designed for CubeSat: Dual feed, L&S dual-band stacked, and circularly polarized," *IEEE Antennas and Propag. Magazine*, vol. 58, no. 3, pp. 16-21, June 2016.
[19] C. X. Mao, S. Gao, Y. Wang, Q. X. Chu, and X. X. Yang, "Dual-Band Circularly Polarized Shared-Aperture Array for C-/X-Band Satellite Communications," *IEEE Trans. Antennas Propag.*, vol. 65, no. 10, pp. 5171-5178, Oct. 2017.
[20] Y. Yang, Y. L. Ban, Q. Sun, and C. Y. D. Sim, "A *X*-/*Ka*-Band Linearly Polarized Low Profile Shared-Aperture Antenna Array for Satellite Applications," *IEEE Access*, vol. 10, pp. 105292-105302, 2022.
[21] T. Lou, X. X. Yang, G. Tan, and S. Gao, "Shared Aperture Dual-Band Dual Circularly Polarized Multibeam Antenna for Satellite-Assisted Internet of Vehicles," *IEEE Internet of Things Journal*, vol. 11, no. 7, pp. 12000-12011, 1 April1, 2024.
[22] S. Ji, Y. Dong, S. Wen, and Y. Fan, "C/X Dual-Band Circularly Polarized Shared-Aperture Antenna," *IEEE Antennas Wireless Propag. Lett*., vol. 20, no. 12, pp. 2334-2338, Dec. 2021.
[23] J. Ran, Y. Wu, C. Jin, P. Zhang, and W. Wang, "Dual-Band Multipolarized Aperture-Shared Antenna Array for Ku-/Ka-Band Satellite Communication," *IEEE Trans. Antennas Propag.*, vol. 71, no. 5, pp. 3882-3893, May 2023.
[24] Y. Dong, R. Xu, Y. H. Yang, and S. G. Zhou, "Compact Shared-Aperture Dual-Band Dual-Circularly-Polarized Waveguide Antenna Array Operating at K/Ka-Band," *IEEE Trans. Antennas Propag.*, vol. 71, no. 1, pp. 443-449, Jan. 2023.
[25] J. Zhu, Y. Yang, Z. Hou, S. Liao, and Q. Xue, "Aperture-Shared All-Metal Endfire High-Gain Parabolic Antenna for Millimeter-Wave Multibeam and Sub-6-GHz Communication Applications," *IEEE Trans. Antennas Propag.*, vol. 71, no. 3, pp. 2784-2789, March 2023.
[26] D. E. Serup, G. F. Pedersen, and S. Zhang, "Dual-Band Shared Aperture Reflectarray and Patch Antenna Array for S- and Ka-Bands," *IEEE Trans. Antennas Propag.*, vol. 70, no. 3, pp. 2340-2345, March 2022.
[27] Y. Yao, X. Q. Lin, T. Qin, Y. Su, and X. Yang, "Shared-Aperture Ka-Band Reflectarray and X-Band Phased Array for Broadband Inter-Satellite Communication," *IEEE Trans. Antennas Propag.*, vol. 70, no. 11, pp. 11199-11204, Nov. 2022.
[28] L. Leszkowska, M. Rzymowski, K. Nyka, and L. Kulas, "High-Gain Compact Circularly Polarized X-Band Superstrate Antenna for CubeSat Applications," *IEEE Antennas and Wireless Propag. Letters*, vol. 20, no. 11, pp. 2090-2094, Nov. 2021.
[29] S. X. Ta, I. Park, "Low-profile broadband circularly polarized patch antenna using metasurface," *IEEE Trans. Antennas Propag.*, vol. 63, no. 12, pp. 5929-5934, Dec. 2015.
[30] L. Xiang, F. Wu, C. Yu, Z. H. Jiang, Yu. Yao, and W. Hong, "A wideband circularly polarized magneto-electric dipole antenna array for millimeter-wave applications," *IEEE Trans. Antennas Propag.*, vol. 70, no. 5, pp. 3876-3881, Dec. 2021.
[31] Q. Tan, K. Fan, W. Yu, W. Wang, L. Liu and G. Q. Luo, "A Circularly Polarized Magneto-Electric Dipole Antenna Array With Wide AR and Impedance Bandwidth for Millimeter-Wave Applications," *IEEE Antennas and Wireless Propag. Letters*, vol. 22, no. 9, pp. 2250-2254, Sept. 2023.
[32] C. Wang *et al*., "Millimeter-Wave Ultra-Wideband Circularly Polarized OMD Antenna Array Based on Dual-Mode Sequential Rotated Feeding," *IEEE Trans. Antennas Propag.*, vol. 71, no. 10, pp. 7824-7836, Oct. 2023.